Research Article

Journal of RAMAN SPECTROSCOPY

Received: 2 May 2008 Accepted: 17 July 2008 Published online in Wiley Interscience: 20 October 2008

(www.interscience.wiley.com) DOI 10.1002/jrs.2093

Direct visual evidence for the chemical mechanism of surface-enhanced resonance Raman scattering via charge transfer

Mengtao Sun,[a*] Shasha Liu,[b,c] Maodu Chen[b,c] and Hongxing Xu[a,d]

We describe the chemical and electromagnetic enhancements of surface-enhanced resonance Raman scattering (SERRS) for the pyridine molecule absorbed on silver clusters, in which different incident wavelength regions are dominated by different enhancement mechanisms. Through visualization we theoretically investigate the charge transfer (CT) between the molecule and the metal cluster, and the charge redistribution (CR) within the metal on the electronic intracluster collective oscillation excitation (EICOE). The CT between the metal and the molecule in the molecule–metal complex is considered as an evidence for chemical enhancement to SERRS. CR within the metal on EICOE is considered as an evidence for the electromagnetic enhancement by collective plasmons. For the incident wavelength from 300 to 1000 nm, the visualized method of charge difference density can classify the different wavelength regions for chemical and electromagnetic enhancement, which are consistent with the formal fragmented experimental studies.

Supporting information may be found in the online version of this article.

Keywords: SERRS; chemical enhancement; charge transfer; charge difference density; intracluster charge redistribution

Introduction

Thirty years after the discovery of surface-enhanced Raman scattering (SERS),[1,2] it is generally accepted that the enormous enhancement of the Raman signal is due to two types of mechanisms.[3] The first is the electromagnetic (EM) enhancement, which is caused by the strong surface plasmon resonance of curved metal surfaces coupled to the incident light.[4–7] The second is the chemical enhancement,[8–29] which can be considered similar to a resonance Raman process between the ground electronic state of the molecule–metal complex and its new excited levels arising from charge transfer (CT) between the metallic surface and the adsorbed molecule. Recently, Sun *et al*.[29] have investigated the surface-enhanced resonance Raman scattering (SERRS) mechanism of the pyridine–Ag_2 complex, in which the CT has been visualized with charge difference density.[30,31] The visualized CT between pyridine and Ag_2 cluster is a direct evidence for chemical enhancement to SERRS. The charge redistribution (CR) within the Ag_2 cluster on the electronic intracluster collective oscillation excitation (EICOE) results in a Förster excitation transfer from the Ag_2 cluster to pyridine. Raman scattering of pyridine via Förster excitation transfer is enhanced by the local EM field (collective plasmon). The Förster excitation in the local EM field enhancement in small clusters is analogous to the plasmon excitation in EM enhancement in large nanoparticles. It should be noted that when the size of the nanoparticles is large enough ($R > 10$ nm), the 'local electromagnetic field enhancement' is called 'electromagnetic enhancement'.[32–34]

Experimentally, Peyser-Capadona *et al*.[35] have shown that small (2–8 atoms) silver clusters enclosed in a dendrimer or peptide scaffold can produce single-molecule Raman scattering characteristic of the scaffold. Jensen *et al*.[21] have investigated theoretically the size dependence of the enhanced Raman scattering of pyridine adsorbed on Ag_n ($n = 2–8, 20$) clusters, and the results showed that both the absorption and Raman scattering properties depend strongly on the cluster size and the adsorption site. Several theoretical studies have revealed that the absorption properties of a 20-atom silver tetrahedral cluster behave quite similar to the plasmon excitation observed in nanoparticles, and the Raman enhancement due to this cluster is comparable to that from large nanoparticles (>10 nm).[19–21] Owing to high computational demands for large clusters, most electronic structure studies have adopted small silver clusters to mimic model surfaces.[19–22,29,36–41] Recent photoelectron spectroscopy and relativistic density functional calculations strongly predict that Au_{20} has a tetrahedral geometry similar to a fragment of bulk face-centered cubic (fcc) gold.[42] In this paper, the tetrahedral Ag_{20} is adopted, which is a relaxed fragment of the fcc lattice of bulk silver and is one of the local minima for the Ag_{20} cluster.[43,44] For this tetrahedral Ag_{20}, there are two very different binding sites (S-complex and V-complex, Fig. 1). The former consists of an on-top binding to one of its four faces, which represents a

* *Correspondence to: Mengtao Sun, Beijing National Laboratory for Condensed Matter Physics, Institute of Physics, Chinese Academy of Sciences, Beijing 100190, P. R. China. E-mail: mtsun@aphy.iphy.ac.cn*

a *Beijing National Laboratory for Condensed Matter Physics, Institute of Physics, Chinese Academy of Sciences, Beijing 100190, P. R. China*

b *School of Physics and Optoelectronic Technology, Dalian University of Technology, Dalian 116024, P. R. China*

c *Department of Chemistry, Dalian University of Technology, Dalian 116024, P. R. China*

d *Division of Solid State Physics, Lund University, Lund 22100, Sweden*

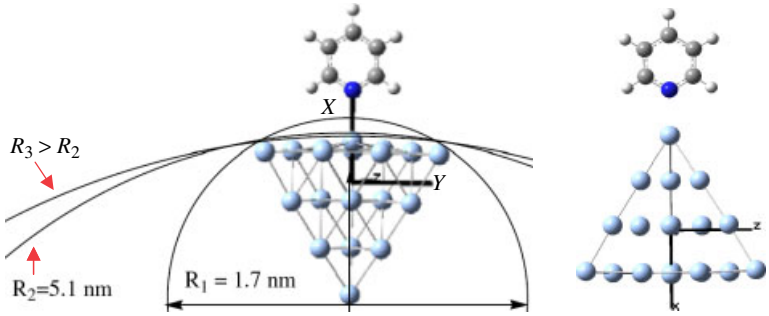

(a) Surface (S) complex (b) Vertex (V) complex

Figure 1. (a) and (b) Configurations of the two pyridine–Ag_{20} complexes having C_S symmetry. This figure is available in colour online at www.interscience.wiley.com/journal/jrs.

(111) surface of fcc silver, while the latter consists of binding to one of its vertices, which represents an ad-atom site.[19] It has been found that the calculated SERS spectrum with the S-complex is in better agreement with the experimental results (for large nanoparticles) than with the V-complex.[19,22] As illustrated in Fig. 1, the tetrahedral Ag_{20} can well mimic a part of large nanoparticles, and that is probably the reason why the S-complex is normally used for SERS calculations for molecules absorbed on metal nanoparticles.

In this paper, we describe the chemical and EM enhancement of SERRS for the pyridine molecule adsorbed on silver nanoparticels, where the S-complex is chosen to mimic nanoparticles of a much larger size than the Ag_{20} cluster. By using visualization methods we theoretically investigate how CT occurs between pyridine and the Ag_{20} cluster, and how CR occurs within the Ag_{20} cluster on the EICOE. The CT between the Ag_{20} cluster and pyridine in the pyridine–Ag_{20} complex is an evidence for chemical enhancement in SERRS. CR within Ag_{20} is an evidence for EM enhancement by collective plasmon excitation in EICOE.

Methods

The ground state geometry of pyridine–Ag_{20} (S-complex) was optimized with density functional theory (DFT)[45] using the B3PW91 functional,[46,47] the LANL2DZ basis set[48] for Ag, and the 6-31G basis set for C, N and H. The SERS of the pyridine–Ag_{20} complex was calculated with the same method as at zero frequency, which is normal Raman scattering (NRS) of the pyridine–Ag_{20} complex. The electronic structures of pyridine–Ag_{20} were carried out by the time-dependent DFT (TD-DFT) method,[49] and the same functional and basis set. For comparison, the ground state geometry of pyridine was optimized with DFT, using the B3LYP functional[50] and the 6-31G basis set, from which the energy levels of the HOMO and the LUMO were obtained. The above-mentioned quantum chemical calculations were performed with the Gaussian 03 suite.[51] The Fermi energy levels of tetrahedral Ag_{20} and the S-complex as well as the energy levels of highest occupied molecular orbital (HOMO) and lowest unoccupied molecular orbital (LUMO) of tetrahedral Ag_{20} were calculated with the DFT method, the local density approximation with the Perdew-Zunger parametrization (LDA-PZ) functional, the double zeta polarized (DZP) basis set and 300 K for electron temperature.The calculations were done with Virtual NanoLab.[52] The charge difference density[29–31] was employed to visualize the CT between pyridine and Ag_{20} cluster, and CR within Ag_{20} cluster in the EICOE.

Table 1. Calculated static electronic polarizability components in a.u. The Cartesian coordinate can be seen from Fig. 1(a)

	xx	yy	zz
Pyridine	63.305	66.190	18.751
S-complex	1101.587	905.737	876.867

Results and Discussion

Ground state properties of pyridine–Ag_{20} complex

Because of the coupling interaction between pyridine and the Ag_{20} clusters, the CT of the complexes (0.166 e is transferred from pyridine to the Ag_{20} cluster) results in a large static electronic polarizability (Table 1). The SERS spectrum at zero frequency can be seen from Fig. 2, which is contributed by the static chemical (SC) enhancement. There are three strongly enhanced modes, 984 cm^{-1} (ring breathing with N moving toward silver), 1064 cm^{-1} (ring breathing) and 1582 cm^{-1} (C–C stretching with the α carbon next to nitrogen vibrating toward the silver cluster), which are symmetric vibrational modes perpendicular the surface (Fig. 2), that is, the orientation of CR between pyridine and the Ag_{20} cluster. So the selection rule for the SC enhancement is that the orientation of CT in the ground state is the same as that of molecular vibrations in the ground state.

The Fermi energy level and the energy levels of HOMO and LUMO for the Ag_{20} cluster can be seen from Fig. 3. According to

$$\Delta E(Ag_{20}) = E_{HOMO}(Ag_{20}) - E_{LUMO}(Ag_{20}) \quad (1)$$

the minimum energy of EICOE is 725 nm for the isolated Ag_{20} cluster. Because of the coupling interaction between pyridine and the Ag_{20} clusters (CT within the complex), the Fermi energy level of the S-complex is slightly increased by 0.027 eV, which was estimated with

$$\Delta E_{Fermi} = E_{Fermi}(\text{S-complex}) - E_{Fermi}(Ag_{20}) \quad (2)$$

The minimum energy of the incident light is ~503 nm for the CT (from Fermi energy level to the LUMO of isolated pyridine)

Journal of RAMAN SPECTROSCOPY

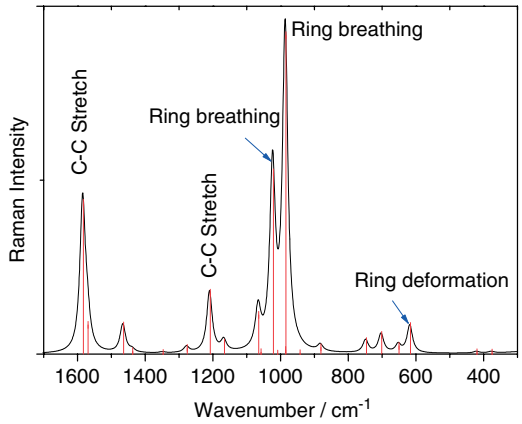

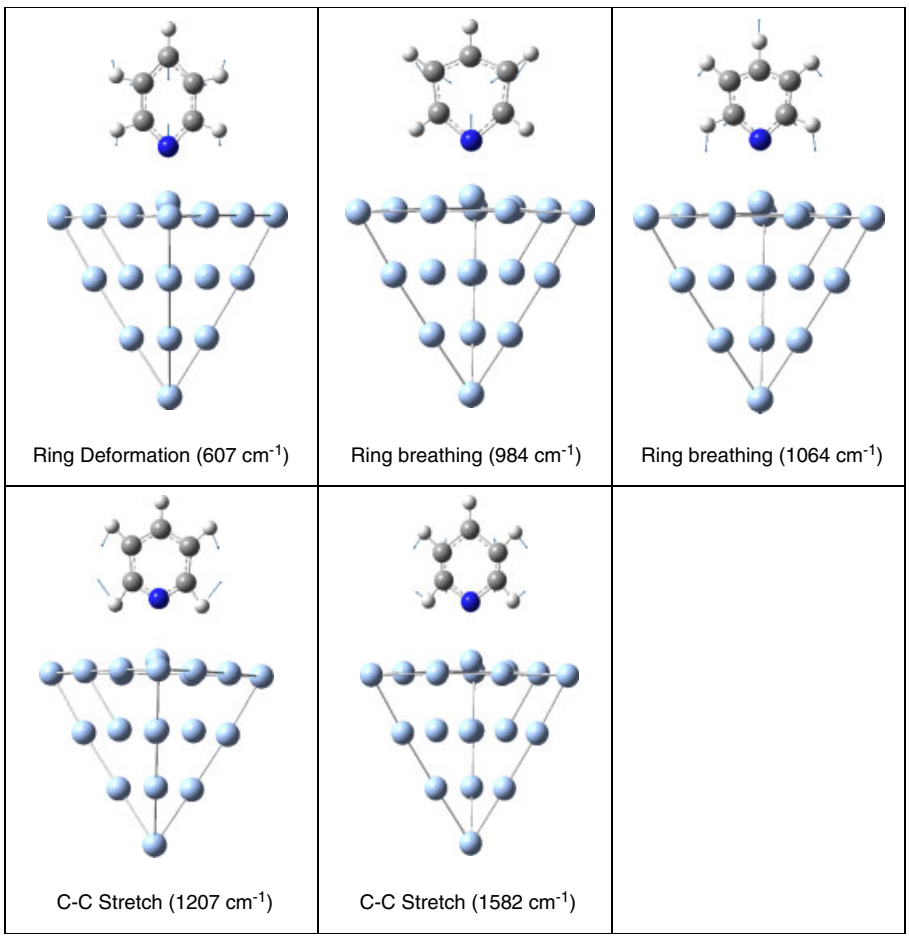

Figure 2. The simulated SERS (normal Raman scattering) spectrum of pyridine adsorbed on large (S-complex) silver nanoparticles. The scale factor of the wavenumbers is set as 0.96 in our calculations. This figure is available in colour online at www.interscience.wiley.com/journal/jrs.

resonant transitions, which was calculated with

$$\Delta E(\mathrm{CT_{min}}) = E_{\mathrm{LUMO}}(\mathrm{pyridine}) - E_{\mathrm{Fermi}}(\mathrm{Ag_{20}}) \quad (3)$$

The CT resonant transitions with large oscillator strength is at ~380 nm, which could be calculated with

$$\Delta E(\mathrm{CT}) = E_{\mathrm{LUMO}}(\mathrm{pyridine}) - E_{\mathrm{HOMO}}(\mathrm{Ag_{20}}) \quad (4)$$

So, a few conclusions can be made: (1) when energy of the incident light is below 1.71 eV (725 nm), there is no resonant electronic state transition, and the Raman scattering is the SERS contribution from SC enhancement; (2) when the energy of the incident light is between 725 and 503 nm, there are resonant electronic state transitions, but the electronic transitions are the EICOE, without CT from Ag_{20} to pyridine, so the SERS is only contributed by the EM enhancement by plasmon excitation; and (3) when the energy of the incident light is larger than that for 503 nm excitation, CT from Ag_{20} to pyridine on the resonant electronic state transitions could occur, which results in chemical

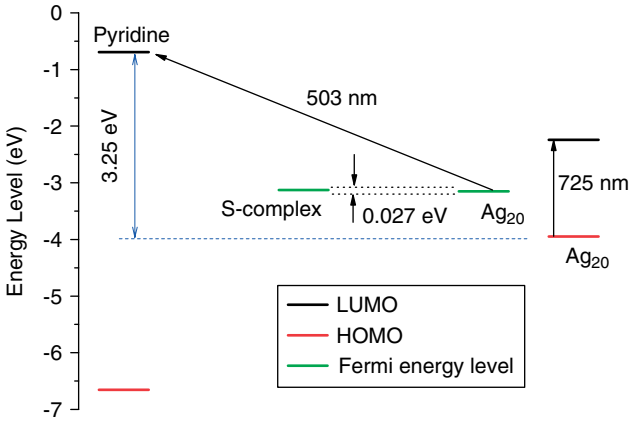

Figure 3. The Fermi energy level and energy levels of HOMO and LUMO for Ag_{20} cluster, the Fermi energy level of S-complex, and the energy levels of pyridine. This figure is available in colour online at www.interscience.wiley.com/journal/jrs.

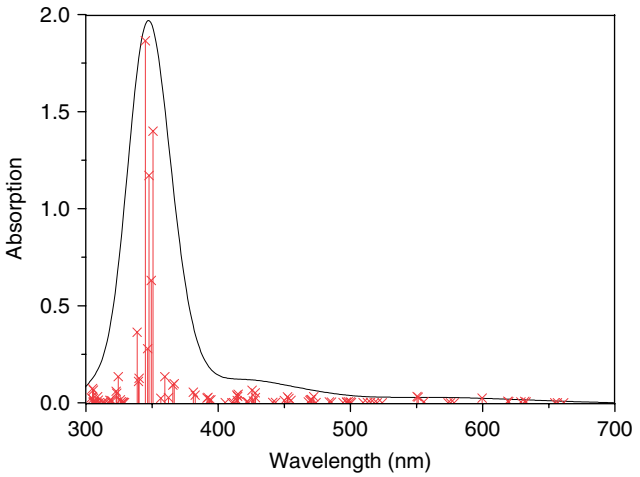

Figure 4. The optical electronic state absorption of the S-complex. This figure is available in colour online at www.interscience.wiley.com/journal/jrs.

enhancement for SERS. When the incident light is of wavelength ~380 nm, there are strong CT excited states (strong CT optical absorption).

Electronic excited state properties of pyridine–Ag_{20} complex

Depending on the nature of the interaction between pyridine and the metal, the new CT (from Ag_{20} cluster to pyridine) excited states or intracluster CR excited states on EICOE can occur, and the enhancement of SERS is roughly proportional to the oscillator strength of the transition.[19] The calculated absorption spectrum with TD-DFT can be seen from Fig. 4, where the lowest resonance energy is at ~670 nm with weak oscillator strength, and the strongest absorption is at ~350 nm. So, if the incident wavelength is above 670 nm (for example, for 780 and 1064 nm excitation), the spectrum is SERS without CT, and the Raman profile of SERS should be similar to the one in Fig. 2. It should be noted that the lowest electronic transition is at 670 nm calculated with TD-DFT method, while the lowest electronic transition is at 725 nm calculated with Eqn (1). The difference in energies (shift corresponds to ~45 nm) results from the different methods we have used. Usually, the band gap calculated with Eqn (1) is slightly lower than the optical electronic state transition energy of S_1 for the LDA functional.[53] It should be noted that the strong CT optical absorption is at ~380 nm calculated with Eqn (4), while the strong optical absorption is at ~350 nm calculated with TD-DFT. This difference results from the different methods we used in the calculations.

Chemical and EM enhancement mechanism of SERS for the S-complex

The SERS at resonance is proportional to the oscillator strength of the electronic state transitions.[19] As shown in Fig. 4, the strongest enhancement for SERS is at ~350 nm. Depending on the CT excited states (from Ag_{20} cluster to pyridine) or the intracluster (Ag_{20} cluster) CR excited states on EICOE at ~350 nm incident excitation, the corresponding SERS enhancement can be characterized as either chemical enhancement or EM enhancement. The charge difference densities for the S-complex at 350 nm with strong oscillator strengths are listed in Fig. S1 in Supporting Information. For the S-complex, almost all the excited states are CT excited states, where electrons transfer from Ag_{20} cluster to pyridine, except for S_{68} (which is an intracluster CR excited state), so SERRS at ~350 nm for the S-complex mainly originates from chemical enhancements via CT from the Ag_{20} cluster to pyridine, while the EM enhancement via intracluster CR on EICOE is very weak.

As mentioned above, the minimum wavelength of the incident light is ~503 nm for the CT (from Ag_{20} cluster to pyridine) resonant transition, according to Eqn (3). If the ~45 nm red shift is considered (discussed above), the lowest Ag_{20} cluster to the pyridine CT excited state calculated with TD-DFT method should be at ~458 nm. By examining the excited state properties of the S-complex with charge difference density (shown in Fig. S1 in Supporting Information), the lowest Ag_{20} cluster to the pyridine CT excited state calculated with TD-DFT method is at ~455 nm. In the region from 455 to 338 nm, almost all the excited states are the CT excited states (from Ag_{20} cluster to pyridine, see Fig. S1 in Supporting Information). So, the SERS in this region should almost be contributed by chemical enhancement via CT from the Ag_{20} cluster to pyridine. From the charge difference density in Fig. S1 (Supporting Information), from 338 to 300 nm, the SERS of pyridine should be contributed by EM enhancement by plasmon excitation since all of these excited states are intracluster CR excited states, except S_{89} at ~318 nm (which is the Ag_{20} cluster to pyridine CT excited state).

In the region from 455 to 670 nm, almost all the excited states are the intracluster CR excited states (electron and hole are localized in the metal cluster; see Fig. S1 in Supporting Information). So, the SERRS in this region should mostly be contributed by EM enhancement via plasmon excitation.

To summarize the different SERS enhancement mechanisms of the S-complex for different incident excitations from 300 to 1000 nm, the spectrum enhancement mechanisms are illustrated in Fig. 5, where CT for chemical enhancement happens roughly in the region of 330–455 nm, and CR for EM enhancement roughly in the regions of 300–330 nm and 455–670 nm. The region of the SC enhancement is above 670 nm.

It is interesting that the formal fragmented experimental studies on SERS of pyridine at different incident wavelengths can actually confirm our results in Fig. 5. Comparing the calculated SERS spectrum of pyridine in Fig. 2 with the experimental SERS spectrum at the incident light of 532 nm,[54] one can find that they have very similar Raman profiles. Since SERS of pyridine at 532 nm

Journal of RAMAN SPECTROSCOPY

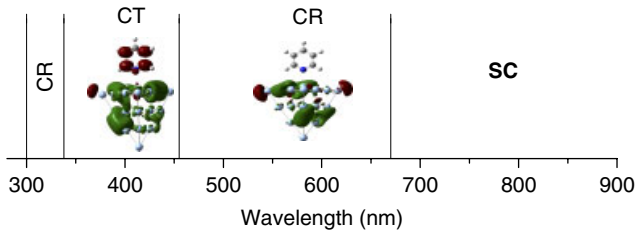

Figure 5. The chemical and electromagnetic field enhancement mechanisms at different wavelength regions. The two inserts are the charge difference densities for the intracluster excitation and CT excitation (charge transfer from Ag_{20} cluster to pyridine), respectively, where the green and the red stand for hole and electron, respectively. This figure is available in colour online at www.interscience.wiley.com/journal/jrs.

is contributed by the EM field enhancement in the enhancement spectrum of Fig. 5, and the EM enhancement should not change the Raman profile, the consistency between the experiment and the simulation can be well explained. Recently, SERS of pyridine adsorbed on the S-complex at the strongest absorption of 350 nm has been calculated by Zhao *et al*.,[19] where the intensities of the ring deformation mode at 607 cm^{-1} was strongly enhanced, while the intensity of ring stretch modes at 1208 cm^{-1} was decreased to very small values. The selective changes of the Raman peaks are the evidence of the chemical enhancement, which is consistent with our conclusions in Fig. 5.

The CT mechanism is also often used to explain the dependence of certain bands in SERS experiments on the electrode potential.[15,16,28] The idea is that by changing the electrode potential, the CT state can be tuned to be at resonance or away from it for certain incident excitation wavelengths. The relationship between the optical absorption energy in the absorption spectrum and the shift of electrode potential can be estimated with

$$E(\Delta V) = E_0(\Delta V = 0) - e\beta\Delta V \quad (5)$$

where $E(\Delta V)$ is the optical absorption energy with ΔV the change of the cathode potential V and $\beta \leq 1$. For pyridine adsorbed on silver nanoparticles, $\beta = 0.75$.[28] According to Eqn (5), the relationship between energy in the absorption spectra and the shift of the electrode potential can be seen from Fig. 6(a) and (b). Experimentally, the ring stretch of the normal mode at 1208 cm^{-1} (the 9a normal mode in Fig. 6(a)) and the ring deformation of the normal mode at 607 cm^{-1} (the 6a normal mode in Fig. 6(a)) have been found to be quite sensitive to the potential of the electrode. The vibrations of these two normal modes can be seen in Fig. 2. In that experiment, the incident light is 514.5 nm, i.e. $E_0(\Delta V = 0) = 514.5$ nm. When the cathode potential is −0.25 V, the incident light of 514.5 nm corresponds to a new incident excitation of 2.66 eV (467 nm). According to the spectrum of the enhancement mechanisms in Fig. 5, the enhancement of SERRS is electromagnetic. So the profile of SERRS of pyridine is similar to the case of zero potential. When the cathode potential is increased to −0.5 V, however, the incident light of 514 nm corresponds to a new incident excitation of 2.91 eV (426 nm). According to the spectrum of enhancement mechanisms in Fig. 5, the enhancement of SERRS now becomes chemical due to CT excitation states. In the experimental SERRS spectrum, the ring stretch modes at 1208 cm^{-1} and the C–C stretching appear with low intensity, which gives evidence for chemical enhancement. This experimental result is again consistent with the conclusion in Fig. 5. With the further increase of the cathode potentials, the intensities of the ring stretch mode at 1208 cm^{-1} and ring deformation mode at 607 cm^{-1} are gradually enhanced, and the strongest enhancement of these two modes is obtained when the potential goes to −1.2 V. This is easily understood. Increasing the cathode potential is equivalent to tuning the energy of the incident light at 514 nm close to the strong optical absorption at 350 nm. When the cathode potential is −1.2 eV, the incident light of the laser corresponds to 370 nm, which is very close to the peak absorption. The changes of the SERRS spectra clearly show the evidence of chemical enhancement, which is consistent with the enhancement spectrum in Fig. 5. Arenas *et al*.[16] have reasoned that the experimental appearance of the modes at 1208 and 607 cm^{-1} on silver electrodes coincides with the appearance of CT. The displacements between the ground state of pyridine and its anion for these two vibrational modes are much larger than others, so relative intensities of SERRS spectra for these two normal modes are strongly enhanced.

If Eqn (5) is rewritten as

$$E_0(\Delta V = 0) = E(\Delta V) + e\beta\Delta V \quad (6)$$

one can consider that the increase of the cathodic potential is not tuned to the energy of the incident light, but shifted the optical absorption from higher energy (eV) toward 514.5 nm.

It should be noted that the calculated SERRS spectra at different incident wavelengths for the pyridine–Ag_2 complex[29] were all contributions from Albrecht's term-A (the Frank-Condon term),[55] since the laser excitation is close to an allowed electronic transition, and only one excited state is involved. With the increase of the cluster size, there are more excited states (the energy levels of electronic states are much closer, see Fig. 4) close to the wavelength of the incident laser, so Albrecht's term-B (Herzberg-Teller term)[55] will also contribute to SERRS because of the coupling effect between excited states. So, the SERRS spectra calculated with a larger cluster size may be more accurately reproduced than that of a small cluster size. Owing to the high computational demands for a large cluster, the SERRS spectra for the pyridine–Ag_{20} complex are not calculated in this paper, which have been done by Zhao *et al*. in Ref. [19].

Conclusions

In summary, we described the chemical enhancement of SERRS via CT from Ag_{20} to pyridine on resonance excitation, and EM enhancement of SERRS via intracluster CR on EICOE. From the ultraviolet to the infrared region, we construct an enhancement spectrum to classify different incident excitation wavelength regions for the dominating chemical and EM enhancements for pyridine absorbed on Ag_{20} cluster in the S-complex. Our conclusion is supported by the formal fragmented experimental and theoretical SERRS studies of pyridine at different incident laser frequencies.

Acknowledgements

This work was supported by the National Natural Science Foundation of China (Grant nos 10625418, 10604012 and 20703064), the Sino-Swedish Collaborations on Nanophotonics and Nanoelectronics (2006DFB02020), the National Basic Research Project of China (Grant nos 2007CB936801 and 2007CB936804), and the 'Bairen' projects of CAS.

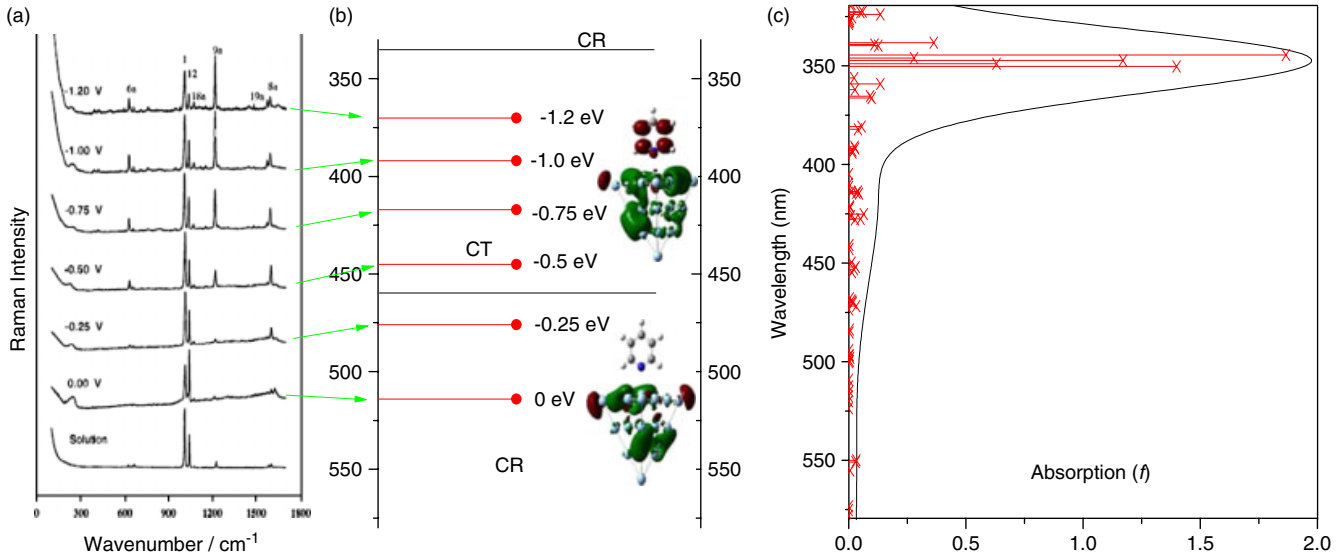

Figure 6. The comparison of absorption spectrum with the tuning of electrode potentials (b), and the SERS of pyridine adsorbed on nanoparticles with different negative electrode potentials. The experimental spectrum (a) is from Ref. [16]. This figure is available in colour online at www.interscience.wiley.com/journal/jrs.

Supporting information

Supporting information may be found in the online version of this article.

References

[1] D. L. Jeanmaire, R. P. Van Duyne, *J. Electroanal. Chem.* **1977**, *84*, 1.
[2] M. G. Albrecht, J. A. Creighton, *J. Am. Chem. Soc.* **1977**, *99*, 5215.
[3] K. Kneipp, H. Kneipp, M. Moskovits (Eds), *Surface-enhanced Raman Scattering, Physics and Applications*, Springer: Heidelberg, **2006**.
[4] M. Moskovits, *Rev. Mod. Phys.* **1985**, *57*, 783.
[5] K. Kneipp, H. Kneipp, I. Itzkan, R. R. Dasari, M. S. Feld, *Chem. Rev.* **1999**, *99*, 2957.
[6] H. X. Xu, E. J. Bjerneld, M. Kall, L. Borjesson, *Phys. Rev. Lett.* **1999**, *83*, 4357.
[7] H. Metiu, P. Das, *Annu. Rev. Phys. Chem.* **1984**, *35*, 507.
[8] A. Otto, *J. Raman Spectrosc.* **2005**, *36*, 497.
[9] A. B. Mayer, *Chem. Rev.* **1996**, *96*, 911.
[10] J. F. Arenas, I. López-Tocón, J. L. Castro, S. P. Centeno, M. R. López-Ramírez, J. C. Otero, *J. Raman Spectrosc.* **2005**, *36*, 515.
[11] P. Kambhampati, C. M. Child, M. C. Foster, A. Campion, *J. Chem. Phys.* **1998**, *108*, 5013.
[12] S. S. Liu, S. B. Wan, M. D. Chen, M. T. Sun, *J. Raman Spectrosc.* **2008**, *39*, 1170.
[13] A. Otto, I. Mrozek, H. Grabhorn, W. Akemann, *J. Phys.: Condens. Matter* **1992**, *4*, 1143.
[14] A. Campion, J. E. Ivanecky, C. M. Child, M. Foster, *J. Am. Chem. Soc.* **1995**, *117*, 11807.
[15] J. F. Arenas, M. S. Woolley, J. C. Otero, J. I. Marcos, *J. Phys. Chem.* **1996**, *100*, 3199.
[16] J. F. Arenas, I. L. Tocón, J. C. Otero, J. I. Marcos, *J. Phys. Chem.* **1996**, *100*, 9254.
[17] J. R. Lombardi, R. L. Birke, T. H. Lu, J. Xu, *J. Chem. Phys.* **1986**, *84*, 4174.
[18] B. N. J. Persson, K. Zhao, Z. Y. Zhang, *Phys. Rev. Lett.* **2006**, *96*, 207401.
[19] L. L. Zhao, L. Jensen, G. C. Schatz, *J. Am. Chem. Soc.* **2006**, *128*, 2911.
[20] L. L. Zhao, L. Jensen, G. C. Schatz, *Nano Lett.* **2006**, *6*, 1229.
[21] L. Jensen, L. L. Zhao, G. C. Schatz, *J. Phys. Chem. C* **2007**, *111*, 4756.
[22] C. M. Aikens, G. C. Schatz, *J. Phys. Chem. A* **2006**, *110*, 13317.
[23] A. M. Michaels, M. E. Nirmal, L. Brus, *J. Am. Chem. Soc.* **1999**, *121*, 9932.
[24] M. J. S. Weaver, S. Farquharson, M. A. Tadayyoni, *J. Chem. Phys.* **1985**, *82*, 4867.
[25] C. Zuo, P. W. Jagodzinski, *J. Phys. Chem. B* **2005**, *109*, 1788.
[26] S. P. Centeno, I. López-Tocón, J. F. Arenas, J. Soto, J. C. Otero, *J. Phys. Chem. B* **2006**, *110*, 14916.
[27] S. Thomas, N. Biswas, S. Venkateswaran, S. Kapoor, S. Naumov, T. Mukherjee, *J. Phys. Chem. A* **2005**, *109*, 9928.
[28] J. F. Arenas, D. J. Fernandez, J. Soto, I. Lopez Tocon, J. C. Otero, *J. Phys. Chem. B* **2003**, *107*, 13143.
[29] M. T. Sun, S. B. Wan, Y. J. Liu, J. Yu, H. X. Xu, *J. Raman Spectrosc.* **2008**, *39*, 402.
[30] M. T. Sun, *J. Chem. Phys.* **2006**, *124*, 054903.
[31] M. T. Sun, P. Kjellberg, W. J. D. Beenken, T. Pullerits, *Chem. Phys.* **2006**, *327*, 474.
[32] A. Campion, P. Kambhampati, *Chem. Soc. Rev.* **1998**, *27*, 241.
[33] A. Otto, Surface enhanced Raman scattering: "classical" and chemical" origins, in *Topics of Applied Physics 54; Light Scattering in Solids*, vol. IV (Ed.: M. G. G. Cardona), Springer: Secaucus, **1984**.
[34] G. C. Schatz, R. P. Van Duyne, Electromagnetic mechanism of surface enhanced spectroscopy, in *Handbook of Vibrational Spectroscopy*, vol. 1 (Eds: J. M. Chalmers, P. R. Griffiths), John Wiley & Sons: New York, **2002**.
[35] L. Peyser-Capadona, J. Zheng, J. L. Gonzalez, T. H. Lee, S. A. Patel, R. M. Dickson, *Phys. Rev. Lett.* **2005**, *94*, 058301.
[36] W. H. Yang, G. C. Schatz, *J. Chem. Phys.* **1992**, *97*, 3831.
[37] R. F. Aroca, R. E. Clavijo, M. D. Halls, H. B. Schlegel, *J. Phys. Chem. A* **2000**, *104*, 9500.
[38] G. Cardini, M. Muniz-Miranda, *J. Phys. Chem. B* **2002**, *106*, 6875.
[39] A. Vivoni, R. L. Birke, R. Foucault, J. R. Lombardi, *J. Phys. Chem. B* **2003**, *107*, 5547.
[40] D. Y. Wu, M. Hayashi, S. H. Lin, Z. Q. Tian, *Spectrochim. Acta, Part A* **2004**, *60*, 137.
[41] P. Johansson, *Phys. Chem. Chem. Phys.* **2005**, *7*, 475.
[42] J. Li, X. Li, H. J. Zhai, L. S. Wang, *Science* **2003**, *299*, 864.
[43] J. L. Wang, G. H. Wang, J. J. Zhao, *Chem. Phys. Lett.* **2003**, *380*, 716.
[44] E. M. Fernandez, J. M. Soler, I. L. Garzon, L. C. Balbas, *Phys. Rev. B* **2004**, *70*, 165403.
[45] P. Hohenberg, W. Kohn, *Phys. Rev.* **1964**, *136*, B864.
[46] A. D. Becke, *Phys. Rev. A* **1988**, *38*, 3098.
[47] J. P. Perdew, J. A. Chevary, S. H. Vosko, K. A. Jackson, M. R. Pederson, D. J. Singh, C. Fiolhais, *Phys. Rev. B* **1992**, *46*, 6671.
[48] P. J. Hay, W. R. Wadt, *J. Chem. Phys.* **1985**, *82*, 270.
[49] E. K. U. Gross, W. Kohn, *Phys. Rev. Lett.* **1985**, *55*, 2850.
[50] C. Lee, W. Yang, R. G. Parr, *Phys. Rev. B* **1988**, *37*, 785.
[51] M. J. Frisch, G. W. Trucks, H. B. Schlegel, G. E. Scuseria, M. A. Robb, J. R. Cheeseman, J. A. Montgomery, T. Vreven Jr, K. N. Kudin,

J. C. Burant, J. M. Millam, S. S. Iyengar, J. Tomasi, V. Barone, B. Mennucci, M. Cossi, G. Scalmani, N. Rega, G. A. Petersson, H. Nakatsuji, M. Hada, M. Ehara, K. Toyota, R. Fukuda, J. Hasegawa, M. Ishida, T. Nakajima, Y. Honda, O. Kitao, H. Nakai, M. Klene, X. Li, J. E. Knox, H. P. Hratchian, J. B. Cross, C. Adamo, J. Jaramillo, R. Gomperts, R. E. Stratmann, O. Yazyev, A. J. Austin, R. Cammi, C. Pomelli, J. W. Ochterski, P. Y. Ayala, K. Morokuma, G. A. Voth, P. Salvador, J. J. Dannenberg, V. G. Zakrzewski, S. Dapprich, A. D. Daniels, M. C. Strain, O. Farkas, D. K. Malick, A. D. Rabuck, K. Raghavachari, J. B. Foresman, J. V. Ortiz, Q. Cui, A. G. Baboul, S. Clifford, J. Cioslowski, B. B. Stefanov, G. Liu, A. Liashenko, P. Piskorz, I. Komaromi, R. L. Martin, D. J. Fox, T. Keith, M. A. Al-Laham, C. Y. Peng, A. Nanayakkara, M. Challacombe, P. M. W. Gill, B. Johnson, W. Chen, M. W. Wong, C. Gonzalez, J. A. Pople, *Gaussian 03, Revision E. 01*, Gaussian: Wallingford, **2004**.

[52] M. Brandbyge, J.-L. Mozos, P. Ordejon, J. Taylor, K. Stokbro, *Phys.Rev. B.* **2002**, *65*, 165401.

[53] S. Tretiak, K. Igumenshchev, V. Chernyak, *Phys. Rev. B* **2005**, *71*, 033201.

[54] J. T. Golab, J. R. Sprague, K. T. Carron, G. C. Schatz, R. P. Van Duyne, *J. Chem. Phys.* **1988**, *88*, 7942.

[55] A. C. Albrecht, *J. Chem. Phys.* **1961**, *34*, 1476.

